Journal of Pharmaceutical and Applied Chemistry

ISSN: 2357-0210 VOLUME 2, ISSUES1, 2016 www.egyptfuture.org/ojs/

Brain Tumor Research in Six Different Maps

Ketevan Kotetishvili * *and Ana Gogishvili.*

Department of Engineering Physics, Georgian Technical University, 77 Merab Kostava Avenue, 0175, Tbilisi. Georgia.

Received: 5 Mar. 2017, Revised: 22 Apr. 2017, Accepted: 25 Apr. 2017.
Published online: 1 May 2017.

Abstract: Paper aims the experimental evaluating of the possibilities of MRI (Magnetic Resonance Imaging) of brain tumors in six different modality maps. Initially, the tumors were discovered on contrast agent enhanced MPRAGE (Magnetization Prepared Rapid Gradient Echo) images. Then, using the obtained MPRAGE information, tumors were located on the six maps, namely: TT (T_2/T_2^*-blood/water signal), SD (Standard Deviation), KP (Kurtosis as width of Peak), FA (Fractional Anisotropy), MK (Mean Kurtosis), and MD (Mean Diffusivity). The highest intensity region of the tumor mass on TT-map was searched and then the intensity values in the same voxel on the rest of the maps were measured. The table of the intensity values for all the 6 maps of all the 44 investigated patients was created and the correlations from these maps were calculated.

Keywords: Brain; Tumors; MRI; TT-, SD-, KP-, FA-, MK-, and MD-maps.

1 Introduction

As is known, the human brain is surrounded by a system of connective tissue membranes called meninges that separate the brain from the skull. This three-layered covering is composed of (from the outside to in) the dura mater ("hard mother"), arachnoid mater ("spidery mother"), and pia mater ("tender mother").

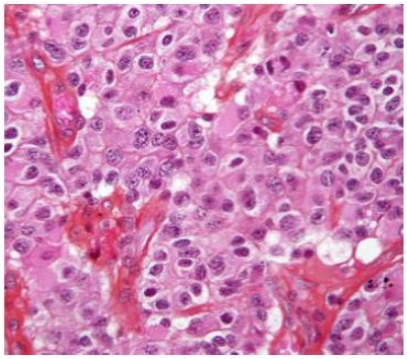

Figure1. Micrograph of a tumor related to oligodendroglia, a type of brain cancer. Brain biopsy.

The cause of many brain tumors is not determined. Risk factors that may occasionally be involved in tumor formation include a number of inherited conditions known as neurofibromatosis, as well as exposure to the industrial chemicals like vinyl chloride, the Epstein–Barr virus, and ionizing radiation as well. While concern has been raised about mobile phone use, the evidences are not clear so far.

A brain tumor or intracranial neoplasm occurs when abnormal cells are formed within the brain. **Figures 1** and **2** show, respectively, cases of oligodendroglia and lung cancer. Treatment may include some combination of surgery, radiation therapy and chemotherapy.

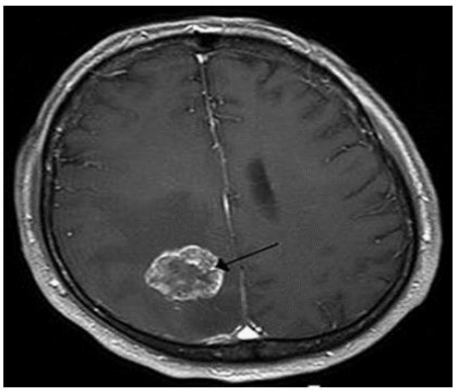

Figure 2. Brain metastasis in the right cerebral hemisphere from lung cancer. Magnetic Resonance Imaging.

Brain tumors have characteristics that allow their malignancy determination and how they will evolve. And determining these characteristics allow the medical team to find its management plan.

For the diagnostic work-up of human brain tumors, the Magnetic Resonance Imaging (MRI) can be considered as a standard approach [1]. It helps in the definition and

ascertaining of tumor extent and indicating its response to treatment. However in some cases, only structural MRI (sMRI) is not sufficient, e.g., the case of differentiation of post-therapeutic scar tissue, tumor rests and tumor recurrence in cerebral gliomasare is challenging.

The diagnostic information obtained using the sMRI may be enriched by other sophisticated MRI techniques such as functional MRI (fMRI), Diffusion Tensor Imaging (DTI), Positron Emission Tomography (PET), multiple-volume proton Magnetic Resonance Spectroscopic Imaging (MRSI), etc. Let's characterize some of them in brief.

DTI can contribute valuable diagnostic information on white matter integrity and fiber tracks [2]. Frequently, diffusion in brain tissue is modeled by that in zeolites. Effect of water adsorption on the thermodynamics and dynamics of the extra-framework cations in zeolite systems was studied in [3]. The binary diffusion coefficients for mixtures in zeolites were determined [4] experimentally by Pulsed Field Gradient (PFG) Nuclear Magnetic Resonance (NMR) method and also theoretically by Molecular Dynamics (MD) simulations. And it was found a good agreement between these two results. Nanostructures can serve for an alternative model of diffusion mechanism. The work [5] represents a review of the available diffusion data for simple metals in nanocrystalline form. It shows that the enhanced diffusion can be modeled in terms of atomic transport along the interfaces. The MD combined with Dissipative Particles Dynamic (DPD) were used [6] to construct a diffusion model of a binary mixture, where the two species differ only in dynamic properties, for which at weak asymmetry the Fikian behavior is observed, but at strong asymmetry the system exhibits non-Fikian (i.e. anomalous) diffusion with sharp front moving with constant velocity. In [7], we have presented the results of pilot study of the correlations between the optimum bias and brain microstructure as revealed by DTI metrics.

The diffusion MRI is known as an important tool in early diagnostics and assessment of stroke. Usually, the Apparent Diffusion Coefficient (ADC) exhibits a strong reduction within the first half an hour after the onset of infarction and allows for a visualization of the ischemic lesion prior to manifestation by other conventional MRI modalities. For the range of low signal of water in the brain tissue as a function of the Diffusion-Weightings (DWs) value can be approximated by a mono-exponential function, under the assumption of a Gaussian diffusion propagator.

A combined measurement of brain perfusion using Diffusion Weighted Imaging (DWI) and oxygen consumption could contribute to the assessment, for example, the clinical relevance of a stenosis in the internal carotid artery. Microstructural features and the physiological state of tissues can be inferred from the DW images.

But for larger values, the deviations from the mono-exponential function become significant and a concept of the ADC becomes insufficient to describe the signal attenuation curve. Recent diffusion MRI studies of stroke in humans have shown that the quantitative parameters characterizing the degree of non-Gaussianity of the diffusion process are much more sensitive to ischemic changes than the ADC. In particular, it was shown that valuable information regarding spatial properties of stroke lesions can be obtained in form of a stratified cortex structure in the lesions that are poorly distinguishable in the ADC-maps. Development of non-Gaussian diffusion imaging is emerging as a novel tool providing clinically useful information on brain tissue [8]. The Diffusion Kurtosis Imaging (DKI) is a novel non-Gaussian method used in such studies.

Additional imaging using PET has been shown [9] to be a powerful tool to resolve some diagnostic deficiencies of conventional MRI. The development of integrated MR–PET hybrid imaging opens up new horizons for imaging in neurooncology. The relationship to structures such as the pyramidal tract to the tumor mass influences the therapeutic neurosurgical approach. Thus, a new generation of imaging systems that combine these two complementary methods is emerging. This combination of two technologies offers complementary diagnostic information for the pre- and post-surgical assessment of brain tumors.

2 Method

For the experimental evaluating of the possibilities of MRI of brain tumors in different maps, initially they were discovered on contrast enhanced Magnetization Prepared Rapid Gradient Echo (MPRAGE) images. It is known that the measurements of the DWI-signal in at least 6 gradient directions are needed for DTI-description of the diffusion behavior in terms of scalar metrics.

Correspondingly, using the MPRAGE information, tumors were located on the six types of maps. Namely, we have chosen:

– TT (T_2/T_2^*-blood/water signal),

– SD (Standard Deviation),

– KP (Kurtosis as width of Peak),

– FA (Fractional Anisotropy),

– MK (Mean Kurtosis), and

– MD (Mean Diffusivity).

Generally, heterogeneous systems, such as tissue, give rise to more than one single diffusion coefficient. It is the reason, why the statistical model of diffusion in biological tissue attributes the distribution to a large number of spin packets each characterized by its individual reduced or apparent diffusivity. Besides, in complex media the measured metrics depends not only upon the genuine features of the underlying microstructure itself but also on the experimental parameters (such as sequence timings). To

keep these factors in mind, the diffusion coefficient evaluated from the pulsed field gradient MRI experiments in brain tissue is conventionally referred to as the ADC.

DTI describes the diffusion behavior in terms such as MD – Mean Diffusivity or FA – Fractional Anisotropy. DKI accounts for deviations from the pattern of Gaussian diffusion by including a second-order term in the Taylor expansion of the natural logarithm of the DW and introduces the parameter KP denoting apparent Kurtosis as width of Peak (Peakedness) for an individual gradient direction. DK determines the initial slope of the signal attenuation curve, while MK – Mean Kurtosis is evaluated as the arithmetic average of KP along various gradient directions.

The correlations calculated according to the obtained maps. In this regard, it should be noted that, the correlation is a statistical measure indicating the extent to which two or more variables fluctuate together. A positive correlation indicates the extent to which those variables increase or decrease in parallel; a negative correlation indicates the extent to which one variable increases as the other decreases and vice versa. In statistics, a perfect positive correlation is represented by the value +1, while the 0 indicates no correlation and the –1 indicates a perfect negative correlation.

3 Results and Discussion

Brain tumors may be presented as a heterogeneous mass (especially after treatment). In particular, the intracranial mass may be heterogeneous and consist of multiple compartments with differing degrees of malignancy. And the maximal metabolic activity lies within the inferior parts of the tumor mass. Imaging helps to identify solid tumor parts in the brain. Differences in the concentrations of contrast agent help to distinguish between them.

Particularly, the diagnostic information on white matter integrity and fiber tracks is too valuable because the fiber tracking provides spatial information on the impairment of vital white fiber tracts, such as the pyramidal tract, by the tumor mass.

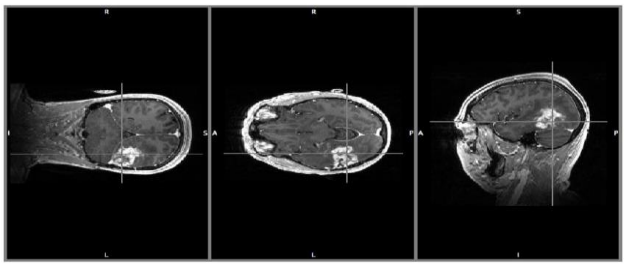

Figure 3. MPRAGE images in slices of the whole brain of a patient.

We discovered tumors on contrast enhanced MPRAGE images (**Figure 3**). Then, using the obtained MPRAGE information, a tumor was located on the above listed 6 maps. The approach provides data of different modalities using the same iso-center. All images are acquired under the similar physiological conditions.

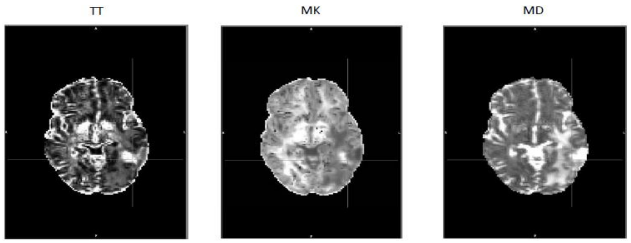

Figure 4. A highest tumor intensity region in a patient's brain according to the multi-modal (TT, MD and MK maps, respectively) assessment of a patient.

Table 1. MRI intensity values for all the maps of all the investigated patients.

Patient	TT_max	SD	KP	FA	MK	MD
FE1-028F-2	3,0916	2,35239	0,578967	0,0837832	1,19225	0,001
FE1-190F	0,135514	0,369849	7,44865	0,120012	0,316004	0,00099
FE1-221M-2	3,65251	2,91045	0,634946	0,0534406	1,04607	0,0013
FE1-223F-5	3,03568	2,48167	0,668306	0,0830468	1,04165	0,0012
FE1-254M	2,45068	2,60488	1,12981	0,226312	0,724239	0,0019
FE1-283M	1,06602	1,1598	1,1837	0,0965109	0,90981	0,0009958
FE1-306M	2,51442	2,91415	1,34323	0,0441735	0,576576	0,0022
FE1-381M	2,02041	2,02195	1,00152	0,260674	0,832707	0,0014
FE1-383F-3	2,76093	2,47687	0,804812	0,161529	0,911527	0,001352
FE1-394F	1,48471	2,23125	2,25847	0,0321731	0,434088	0,0025
FE1-439M	2,30611	2,49191	1,16856	0,0709663	0,698257	0,0018
FE1-440F	2,3842	2,69003	1,273	0,182244	0,617976	0,002
FE1-444M	3,69021	2,95438	0,640958	0,0593818	1,02298	0,0013
FE1-448F	2,66332	2,27161	0,727482	0,102234	1,02039	0,0012
FE1-451M	2,09649	2,59739	1,53492	0,0476915	0,547328	0,0022
FE1-452M	1,56E+00	2,188	1,96187	0,134397	0,481626	0,0023
FE1-454M	1,53262	2,22313	2,10407	0,137249	0,457115	0,0024
FE1-454M-2	0,111182	1,95877	2,31392	0,11182	0,443037	0,0023
FE1-455F-2	1,80986	2,18201	1,45353	0,0811555	0,597606	0,0018
FE1-458F	2,28321	2,55479	1,25205	0,0417414	0,629179	0,0018
FE1-461M-BI	2,32139	2,8094	1,50581	0,0994808	0,563922	0,0023
FE1-469M	1,64654	2,19946	1,78439	0,0723814	0,510284	0,0021
FE1-485F	3,37868	2,46154	0,530787	0,06366985	1,26359	0,001
FE1-491F	2,76243	2,82463	1,04554	0,0672624	0,70401	0,0018
FE1-513M	3,5431	2,83714	0,641203	0,0555112	1,03377	0,0012727
FE1-516M-3	0,438633	0,677127	2,38307	0,0961768	0,667769	0,00096
FE1-542F	1,22835	1,30519	1,12902	0,105947	0,897682	0,0011
FE1-559M	4,29969	2,76103	0,412352	0,0680866	1,48427	0,0009256
FE1-565M	1,92837	2,17205	1,26869	0,0664602	0,664048	0,0017
FE1-575F-2	0,0813092	2,56294	1,10475	0,0813092	0,697989	0,0017
FE1-596M	2,58461	2,09605	0,657677	0,123651	1,12543	0,001
FE1-602F	2,8022	2,48666	0,7841	0,199361	0,947333	0,0014
FE1-607M	2,34411	1,94575	0,688997	0,0600707	1,10114	0,001
FE1-632M-2	2,57152	2,86305	1,23959	0,124451	0,646612	0,0022
FE1-647F	2,51083	2,48069	0,976135	0,0997204	0,80104	0,0016
FE1-652M	1,86965	2,46555	1,73904	0,197238	0,513329	0,0023
FE1-696M	1,33447	2,12548	2,53684	0,0373648	0,407405	0,0026
FE1-720F	3,04621	2,84882	0,8746	0,0376458	0,805833	0,0016
FE1-728M	1,35256	1,6066	1,41091	0,0885885	0,698848	0,0014
FE1-755M	3,67583	2,50214	0,463356	0,0804346	1,38899	0,00092
FT4-036F-7	0,44234	1,19591	8,5653	0,0913357	0,338488	0,0037509
FT4-047M-4	2,96811	2,68919	0,820887	0,0669893	0,864816	0,0015
FT4-471M-2	1,4089	1,69092	1,44042	0,337565	0,691864	0,0015
FT4-495M-3	1,34369	1,64278	1,49473	0,0987241	0,65713	0,0015

Table 2. Correlations between variables calculated according to maps of patients' brains.

	FA	KP	MD	MK	SD	TT
FA	1	0.030590692	-0.0074047	-0.09437393	-0.19731264	-0.18215881
	NaN	0.840062566	0.961047092	0.532722983	0.18871996	0.225654433
KP	0.030590692	1	0.499473245	-0.61589473	-0.6208443	-0.62506933
	0.840062566	NaN	0.000409597	5.21E-006	4.16E-006	3.42E-006
MD	-0.0074047	0.499473245	1	-0.76180258	0.097770505	-0.38309424
	0.961047092	0.000409597	0	7.82E-010	0.518011188	0.008592414
MK	-0.09437393	-0.61589473	-0.76180258	1	0.299737964	0.734176713
	0.532722983	5.21E-006	7.82E-010	0	0.042993887	6.39E-009
SD	-0.19731264	-0.6208443	0.097770505	0.299737964	1	0.739285411
	0.18871996	4.16E-006	0.518011188	0.042993887	NaN	4.42E-009
TT	-0.18215881	-0.62506933	-0.38309424	0.734176713	0.739285411	1
	0.225654433	3.42E-006	0.008592414	6.39E-009	4.42E-009	0

Note that, MK or mean kurtosis can be considered as a measure of the "tailedness" of the probability distribution

of a real-valued random variable. As for the MD or mean diffusivity, it reflects the average magnitude of molecular displacement by diffusion. The more the MD value, the more the isotropic is the medium. TT-signal means something close to diffusion. SD is a measure that is used to quantify the amount of variation or dispersion of a set of data values. KP reflects that in isotropic non-confined media, when the diffusion is described by the Gaussian propagator. FA reflects the directionality of molecular displacements by diffusion and vary between limits of 0 (isotropic diffusion) and 1 (infinite anisotropic diffusion).

The highest intensity region of the mass on TT maps searched and then the intensity values in the same voxel on the rest of the maps measured. Snapshots of MD, MK and TT maps demonstrating the region of interest to measure were made. The images in **Figure 4** represent one and same patient's highest tumor intensity region of the mass on TT, MD and MK maps.

The detailed information can be gathered from the analysis of the obtained maps.

The imaging was approved within the framework of a clinical trial. Here we report the results of 44 patients, all of which gave informed consent before joining the trial.

The intensity values for all the maps of 44 investigated patients were determined. These results are summarized in the **Table 1**.

The **Table 1** was created for comparing the intensity values for all 6 maps of 44 patients. There are 3 groups of cases. Orange color represents the cases when TT is high and MK is low, yellow color means that TT and MK are mainly similar, and lilac color represents the cases when TT is low and MK is high. The 95 % of patients were of high grade (3 – 4) that means that tumor inside is something necrotic and there is a high diffusivity.

The correlations calculated according to the obtained maps are presented in **Table 2**.

4 Conclusions

In summary, the MRI of brain tumors was utilized in six modality maps such as TT, SD, KP, FA, MK, and MD. Initially, the tumors were discovered on contrast agent enhanced MPRAGE mages and then were located on the mentioned maps. The highest intensity region of the tumor mass on TT-map was searched and then the intensity values in the same voxel on the rest of the maps were measured. In total, there were investigated the brains of 44 patients and from these examples the calculated correlations were provided.

Thus, we show the multimodal results demonstrating the feasibility of the MRI and its potential for clinical application in brain tumor patients. Development of diffusion imaging seems to be emerging as a tool providing clinically useful information on brain tissue. Diagnostic performance of MRI-approaches for typing and grading of brain tumors is evaluated as prospective.

Acknowledgement

This paper has been presented at the 4th International Conference "Nanotechnologies", October 24 – 27, 2016, Tbilisi, Georgia (Nano – 2016).

References

[1] D. K. Jones. *Diffusion MRI: Theory, Methods, and Applications.* Oxford, Oxford Univ. Press (2011).

[2] P. J. Basser, D. K. Jones. Diffusion-tensor MRI: Theory, experimental design and data analysis – A technical review. *NMR Biomed*. **15** 456-467 (2002).

[3] B. Coasne, G. Maurin, A. Nicolas, S. Devautour–Vinot, J.-Ch. Giuntini, F. Henn. Effect of water adsorption on the thermodynamics and dynamics of the extra-framework cations in zeolite systems. *Diffusion Fundamentals* **2**, 13.1-13.2 (2005).

[4] Q. Zhao, Sh. Chempath, R. O. Shnurr. Determining binary diffusion coefficients for mixtures in zeolites from PFG NMR, MD simulation and theory. In: *Diffusion Fundamental*s (Eds. J. Karger, F. Grinberg, P. Heitjans). Leipzig, Leipzig Univ. Press, 182-183 (2006).

[5] A. V. Chadwik. Diffusion in nanocrystalline solids. In: *Diffusion Fundamental*s (Eds. J. Karger, F. Grinberg, P. Heitjans). Leipzig, Leipzig Univ. Press, 180-181 (2006).

[6] J. Yaneva, B. Durweg, A. Milchev. Non-Fikian interdiffusion of dynamically asymmetric species: A molecular dynamics study. In: *Diffusion Fundamental*s (Eds. J. Karger, F. Grinberg, P. Heitjans). Leipzig, Leipzig Univ. Press, 180-181 (2006).

[7] K. Kotetishvili, N. Kobalia, F. Grinberg, E. Farrher. Pilot Study of the correlations between the optimum bias and brain microstructure as revealed by DTI metrics. In: Abs. 4th Ann. Retreat Inst. Neurosci. & Med., Jülich, INM, 75-75 (2015).

[8] F. Grinberg, E. Farrher, L. Ciobanu, F. Geffroy, D. Le Bihan, N. J. Shah. Non-Gaussian diffusion imaging for enhanced contrast of brain tissue affected by ischemic stroke. *PLoS One* **9**, e89225 (2014).

[9] I. Neuner, J. B. Kaffanke, K.-J. Langen, E. R. Kops, L. Tellmann, G. Stoffels, Ch. Weirich, Ch. Filss, J. Scheins, H. Herzog, N. J. Shah. Multimodal imaging utilizing integrated MR–PET for human brain tumor assessment. *Eur. Radiol.* **22** 2568-2580 (2012).